small methods
www.small-methods.com

Multiscale 3D Bioprinting by Nozzle-Free Acoustic Droplet Ejection

*Stefan Jentsch, Ramin Nasehi, Christoph Kuckelkorn, Benedikt Gundert, Sanja Aveic, and Horst Fischer**

Bioprinting allows the manufacture of complex cell-laden hydrogel constructs that can mature into tissue replacements in subsequent cell culture processes. The nozzles used in currently available bioprinters limit the print resolution and at dimensions below 100 µm clogging is expected. Most critically, the reduction of nozzle diameter also increases shear stress during printing. At critical shear stress, mechanical damage to printed cells triggers cell death. To overcome these limitations, a novel 3D bioprinting method based on the principle of acoustic droplet ejection (ADE) is introduced here. The absence of a nozzle in this method minimizes critical shear stress. A numerical simulation reveals that maximum shear stress during the ADE process is 2.7 times lower than with a Ø150 µm microvalve nozzle. Printing of cell clusters contained in droplets at the millimeter length scale, as well as in droplets the size of a single cell, is feasible. The precise 3D build-up of cell-laden structures is demonstrated and evidence is provided that there are no negative effects on stem cell morphology, proliferation, or differentiation capacities. This multiscale acoustic bioprinting technique thus holds promise for cell-preserving creation of complex and individualized cell-laden 3D hydrogel structures.

Recent advancements in tissue engineering and printing technology have opened numerous possibilities for moving traditional 2D in vitro cell culture systems toward more robust tissue-like structures. These 3D models, in which subsets of one or more cell types actively interact with a local microenvironment, allow closer approximation to native tissues. In this way, numerous cell features that sustain specific cell functionalization, including polarity, stemness, and migration, as well as the genetic landscape, resemble more closely their (patho) physiological in vivo analogues.[1] Bioprinting methodology has become an integral part of the manufacture of 3D models since it ensures finely tuned spatiotemporal control of cell positioning. 3D bioprinting thus allows the fabrication of complex, multicell-laden constructs while respecting pre-defined tissue architecture and geometry at the micrometer scale.[2]

The most commonly used 3D bioprinting technologies currently are inkjet, microextrusion, and laser-assisted bioprinting.[3] Inkjet printing is a drop-on-demand (DoD) technique and, along with microextrusion, is also a nozzle-based method. In inkjet printing, a controlled volume is compressed by piezoelectric or thermal forces to generate drops through a nozzle. The thermal inkjet process for bioprinting has several key advantages, namely high printing speed, low performance costs, and the wide availability of printers. Its disadvantage, however, is that the printed cell-laden material is subjected to increased thermal and mechanical stress.[3] The microextrusion technique enables the printing of materials of high viscosity and cell density. However, the cell survival rate is lower compared to inkjet-based bioprinting.[4,5] Moreover, it is directly dependent on the needle diameter and inversely correlates with the extrusion pressure.[4–7] Therefore, achieving sufficient cell viability requires low extrusion pressure and a large needle diameter, making the printing process slow and decreasing the resolution.

The only established printing technique that does not require a nozzle is the laser-induced forward transfer method (LIFT). In this process, a laser is used to extract minute amounts of cell-loaded hydrogel material from a substrate and to transfer it to a collector layer.[8–10] Although LIFT is a nozzle-free technique that does not harm cells by shear stress, hitting the substrate layer with the laser beam results in a release of metal particles that can endanger the cytocompatibility of the process.[11] The LIFT method is also subject to restrictions related to laser safety and has limited upscaling potential, making the production of 3D tissue structures on a milli- or even centimeter scale challenging.[12]

However, the nozzle-based printing methods also have limitations due to the nozzles themselves restricting the print resolution. Even if very small nozzles with orifice diameters at the small two-digit micrometer length scale are used,[13] frequent clogging occurs when cell-laden bioinks are processed.[14] In addition, the shear stress on the cells increases significantly with reduction of

S. Jentsch, R. Nasehi, C. Kuckelkorn, B. Gundert, Dr. S. Aveic, Prof. H. Fischer
Department of Dental Materials and Biomaterials Research
RWTH Aachen University Hospital
Pauwelsstrasse 30, 52074 Aachen, Germany
E-mail: hfischer@ukaachen.de

The ORCID identification number(s) for the author(s) of this article can be found under https://doi.org/10.1002/smtd.202000971.

DOI: 10.1002/smtd.202000971

the nozzle diameter. At critical shear stress, the printed cells are damaged and cell death is irreversibly triggered.[3]

To overcome these limitations, the acoustic droplet ejection (ADE) method, which is categorized as a droplet-based bioprinting technique,[14] was evaluated in the present work for its suitability to build a 3D cell-loaded structure without damaging the cells. However, to date only single layers of bioinks have been printed using ADE. Only 2D patterns of separate cell-containing droplets or multiplexed cell cocultures have been successfully achieved.[15,16] The ADE method was initially developed for paper printing or dispensing organic polymers in semiconductor manufacturing. ADE has been commercially available for two decades as a component of a standalone instrument (Echo Liquid Handler, Beckman Coulter) for transfer of low nanoliter volumes between microplates.[17] Its function focuses on automated liquid handling solutions for high throughput screening. Previous studies have adopted an ADE setup for single layer cell application[18] and further development of the ADE principle has made micropatterning possible for the cocultivation of several cell types.[16]

The ADE technique produces a droplet release at an air–liquid interface (ALI) from an open liquid-containing reservoir, and these droplets can be generated across a wide frequency bandwidth. The droplet size is inversely proportional to the frequency of the ultrasonic signal, i.e., the higher the frequency of the ultrasonic signal, the smaller the diameter of the detached droplets. The frequency tunability encompasses more than two decades in the ultrasonic range, extending the range of producible droplet diameters across three orders of magnitude (from 10 µm to 1 mm).[19–21] Considering typical sound velocities in the range of 1–2 km s^{-1} in fluids the typical frequencies range from 1 to 200 MHz, therefore the excitation times range from microseconds to half a millisecond to generate droplets in the sub-picoliter to microliter range.[19,20,22,23]

ADE differs from the piezoelectric inkjet bioprinting technique, where a piezo crystal is deformed inside a chamber and the deformation at 15–25 kHz pushes a droplet through a nozzle.[24] The ADE method, however, uses an open-pool nozzle-free system at 1–200 MHz. More precisely, the ADE method uses the acoustic radiation force of an ultrasonic field to transmit a force to the fluid, i.e., printing medium.[25–27] Another acoustic approach for biofabrication is the use of acoustic waves for cell patterning and cell levitation inside a fluid. Recent publications have demonstrated this biofabrication technology under contactless, rapid, and mild culture conditions.[28–30]

In the study presented here, the ultrasonic field is generated by a spherical piezoelectric crystal commonly known as a high intensity focused ultrasound (HIFU) transducer. A spherical HIFU transducer has also been used in multiplexed cell cocultures and is a component of a commercial liquid handler.[16,17] The focus of the ultrasonic signal must be close to the ALI as this is the site of the highest beam energy density. At this specific region, the acoustic streaming effect occurs and a flow against the surface develops forming a dome on the liquid surface. If the sound pressure of the ultrasonic field and its resulting kinetic flow energy overcome the interface energy of the liquid, an amount of liquid is ejected at the top of the dome in accordance with Rayleigh–Taylor instability.[31] This liquid droplet moves upward and can be collected by a target plate placed in its flight path (**Figure 1**). This bottom-up printing approach taken here exploits gravitational force to reduce the adverse effects of the cell-laden droplet when it makes contact with the platform. This approach also avoids the compression of hanging droplets placed on the printing platform associated with commonly used bioprinting, which causes loss of the 3D shape before the gelling process of the cell-laden hydrogel is complete. The nozzle-free technique makes the acoustic method optimal for dispensing cells since high shear stresses can be avoided, even on very small droplets.

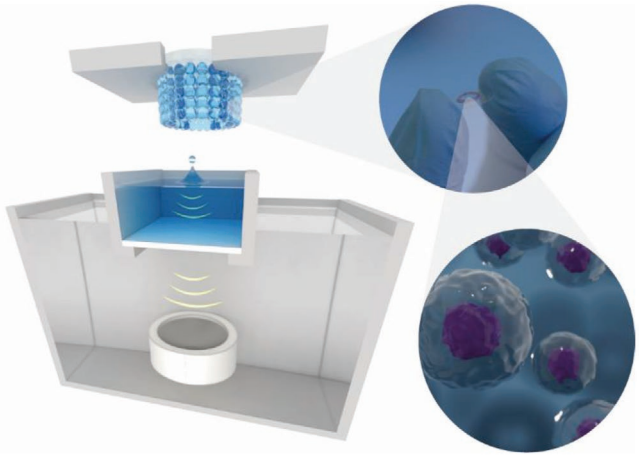

Figure 1. Schematic representation of the acoustic droplet ejection (ADE) 3D bioprinting process. The transducer emits an ultrasonic signal that travels through a water tank, then the bottom of a small coupled reservoir filled with a cell-laden hydrogel suspension, and finally generates an ejection of a cell-laden droplet. The droplet travels upward and attaches to the movable building platform. A small cylinder built from numerous gelled cell-laden hydrogel droplets is demonstrated as a printed 3D component.

In this work, a custom-made printer based on the ADE principle was designed to meet the experimental requirements in order to evaluate its suitability for 3D bioprinting. The acoustic bioprinter setup (Figure S1, Supporting Information) incorporates six separately controllable and movable axes, specifically two sets of three orthogonally arranged axes, one designed to move the building platform and the other the ultrasonic transducer. The transducer centered beneath the bioink reservoir is aligned in height so that the focus point of the ultrasonic signal is set to the ALI. The bioink reservoir is fixed within a tank of water, which acts as a coupling medium that transfers the ultrasonic waves from the transducer to the bioink. This setup allows the emitted ultrasonic signal to eject a droplet from the bioink in the direction of the opposite-facing building platform for the assembly. To build up a 3D cell-laden hydrogel structure, the position of the platform can be adjusted in three spatial directions in order to catch the droplet at predefined positions. A sine wave was generated by a waveform generator (33621A, Keysight). The high frequency signal was then amplified by 50 dB using a Class A power amplifier (A075, Electronics and Innovation) and the inverse piezoelectric effect generated an ultrasonic field through the HIFU transducer (Cnir Hurricane Tech).

The advantage of ADE in enabling variable droplet sizes over more than three size scales has been confirmed in this work and elsewhere. ADE enables multiscale bioprinting, meaning

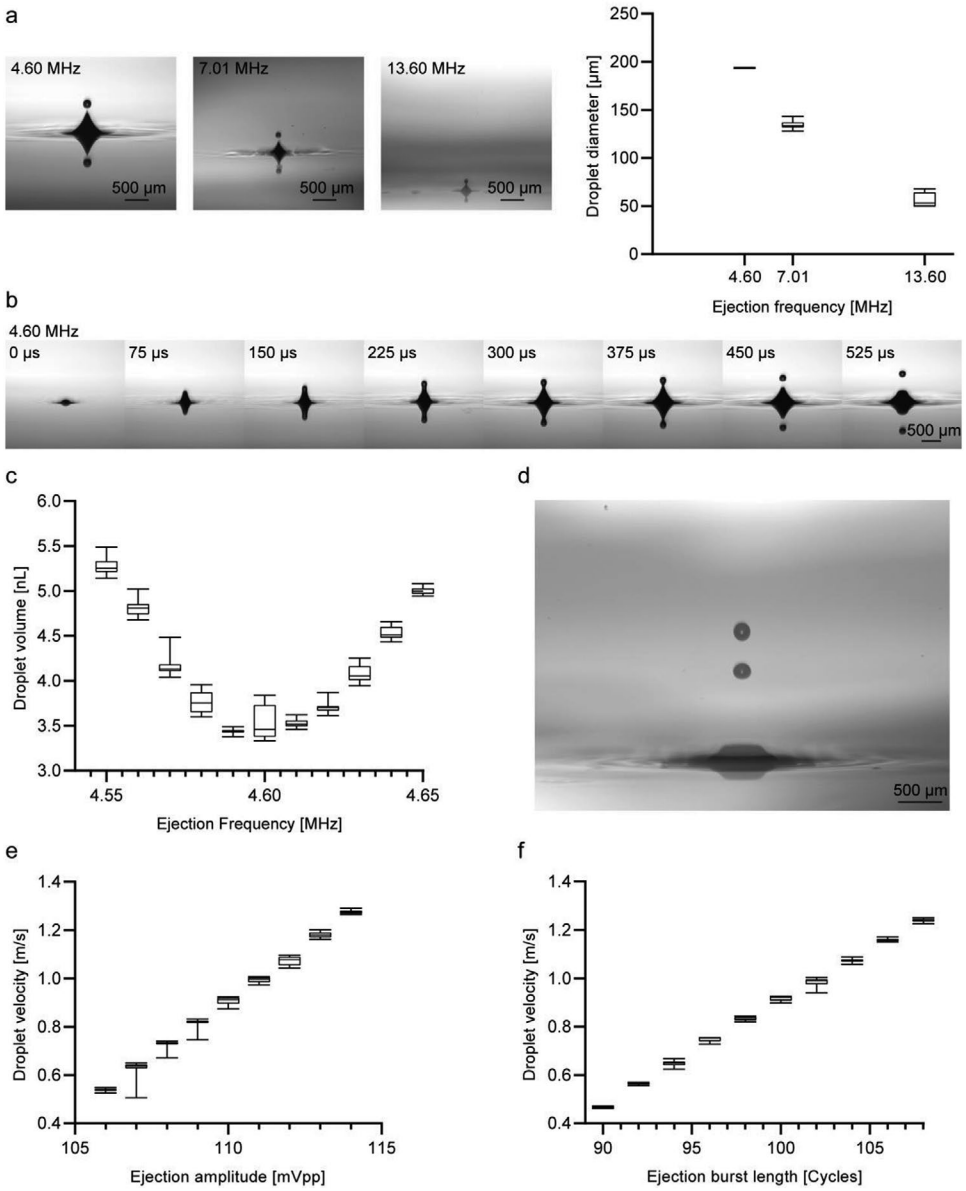

Figure 2. Droplet characteristics depending on the ultrasonic parameters. a) Droplet diameter as a function of the acoustic frequency (left). Boxplot: Measured droplet diameter at different ultrasonic frequencies (right). b) Process of droplet ejection at different time points. The time delay between each image is 75 µs, from 0 µs (left) to 525 µs (right). c) Boxplot: Effect of the frequency near the nominal resonance frequency of the transducer on the droplet volume. d) Double exposure image of the droplet ejection with a time delay of 500 µs between two stroboscopic flashes. e) Boxplot: Droplet velocity showing a linear increase in line with the increase of the ultrasonic ejection amplitude. f) Boxplot: Droplet velocity showing a linear increase in line with the increase of the ultrasonic ejection burst length.

that a range from larger cell aggregates to single cells can be printed precisely in 3D across the scales. In this way, the decreased focal size of the HIFU transducer at higher frequencies results in the ejection of smaller droplets. On the one hand, the 3D structure can be printed as precisely as required or, on the other hand, as imprecisely as possible in order to speed up the overall time for a printing job.

The effect of different ultrasonic parameters on the droplet size and flight velocity was evaluated using a camera system with flash illumination (**Figure 2**). In bioprinting, these evaluations are important since they enable minimization of the required acoustic power for ejection, precise control of a predefined droplet size, and careful adjustment of the platform position to catch the drop while avoiding splashing. In agreement with both the theoretical implications and experimental reports,[20,21,25] the inversely proportional dependence of droplet size on transducer frequency was observed using three different frequencies (4.6, 7.01, and 13.6 MHz) (Figure 2a). Average droplet diameters of 54–183 µm were generated using these three frequencies. Smaller droplets at higher frequencies are generally possible utilizing higher harmonics but transferring a sufficient amount of power through

the transducer, handling a smaller focus region, and avoiding external influences are challenging. The time-lapse images of the liquid surface show the different phases of the droplet ejection (Figure 2b). For each transducer, the droplet size and the droplet velocity vary with the signal amplitude, duration, and variation of its frequency slightly beyond the transducer's nominal resonance frequency. The effect of adjusting the frequency near to nominal resonance frequency shows a behavior with a local minimum droplet volume of ≈3.44 nL considering constant amplitude and excitation duration of the ultrasonic signal (Figure 2c). The volumes are calculated from the measured cross-section, assuming a spherical shape. Based on this calculation, the sphere-equivalent diameters of the drops range from 185 to 219 µm. This interesting phenomenon could originate from the acoustic field and the kinetic energy causing the droplet to detach. However, further investigations are needed to clarify these interactions with certainty. The droplet velocity was determined by the camera system using a double exposure with two light flashes (Figure 2d). Using the droplet velocity, the droplet diameter and water at standard conditions, the Weber number was calculated as 2.19 for the bigger droplets at 4.6 MHz and as 1.23 for the smaller droplets at 13.6 MHz. By adjusting the amplitude and excitation duration of the ultrasonic signal, the speed can be precisely adjusted (Figure 2e,f). This is desirable because accuracy is important for the bioprinting procedure.

To benchmark ADE as an up-and-coming bioprinting technology, a numerical simulation model based on finite element method (FEM) was performed to determine the shear stress on the cell-laden droplets during printing. The results were compared with a numerical simulation of the nozzle-based DoD printing method, which is extensively used in bioprinting.[32–35] Specifically, for the ADE a cylindrical simulation domain of the bioink at the reservoir, and for the DoD the geometry of a commercial microvalve used in previous experiments (SLMD 300G-Ø150 µm, Fritz Gyger) was measured (**Figure 3**).[33,36] The ADE model is based on the Navier–Stokes equations governing the fluid flow with an additional acoustic force term. The acoustic force was modeled based on a constant amplitude A, a shape function $I(x, y, z)$, and its direction $\hat{e}$ as

$$F_{\text{ac.}}(x,y,z) = A \cdot I(x,y,z) \cdot \hat{e} \tag{1}$$

The amplitude of the acoustic force can be written as

$$A = \frac{4\alpha P_{\text{ac}}}{c\pi R_{\text{t}}^2} \tag{2}$$

where P_{ac}, α, c, and R_{t} are the acoustic power, acoustic attenuation, sound velocity, and transducer radius, respectively.[37] This model has been previously used for an acoustically driven cavity flow and validated experimentally for flat transducers.[37,38] To describe the acoustic force distribution for a spherical HIFU transducer, a 3D Gaussian function matches fairly well with the experimental measurements (Figure S2, Supporting Information). Hence, an idealized shape function in the form of

$$I(x,y,z) = e^{-\left(\left(\frac{x-x_0}{a_x}\right)^2+\left(\frac{y-y_0}{a_y}\right)^2+\left(\frac{z-z_0}{a_z}\right)^2\right)} \tag{3}$$

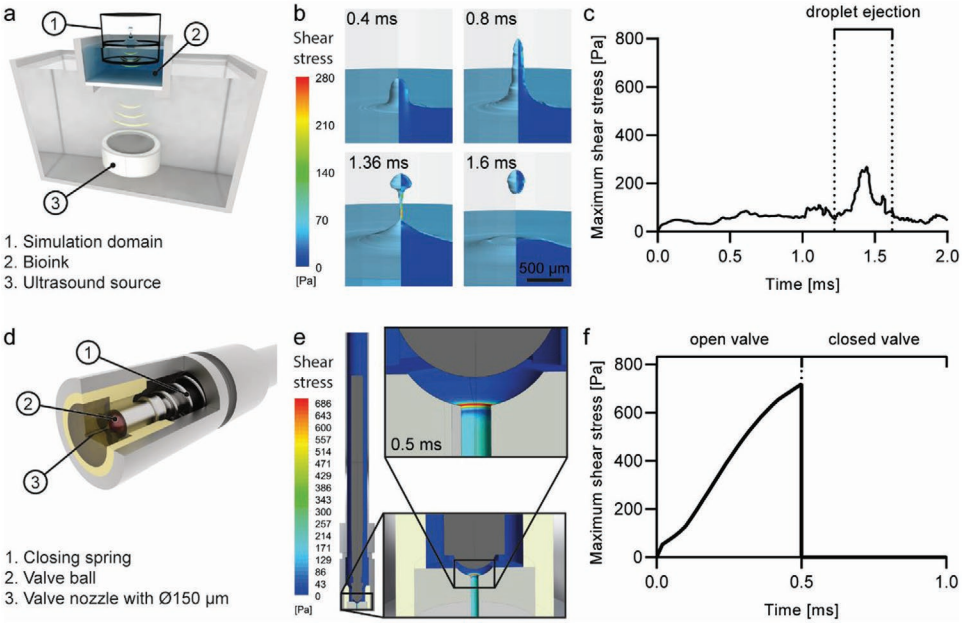

Figure 3. Numerical simulation of acoustic droplet ejection (ADE) and drop-on-demand (DoD) printing techniques using finite element method. The simulation reveals the printing-related shear stress of both methods. a) Schematic representation of the ADE setup and the simulation domain. b) Contour plot of shear stress induced during ADE printing at four time points (0.40, 0.80, 1.36, and 1.60 ms). c) The maximum shear stress over time during the ejection phase of a single droplet using ADE. d) Rendering of the microvalve geometry used for the simulation of DoD. e) Contour plot of shear stress at internal nozzle wall of the microvalve at the end of the valve opening phase (0.5 ms). f) The maximum shear stress over time during the ejection phase of a single drop using DoD. The flow rate drops suddenly to zero resulting in no shear stress when the valve is completely closed. Same scale is used for vertical axis of graphs (c) and (f) to better visualize the much higher level of shear stress during DoD.

was considered for acoustic force distribution, where (x_0, y_0, z_0) is the coordinate of the transducer focus point. Comparing the shapes of the droplet formation between experiment (Figure 2b and Video S1, Supporting Information) and simulation (Figure 3b and Video S3, Supporting Information) qualitatively, the simulation results highly accurately predicted the dynamics of droplet ejection. There is only a slight difference in timing, hence the model is capable of determining the induced shear stress during the ADE process.

Assuming the ejection of a 300 µm diameter water drop with a volume of ≈14 nL, the kinetic energy required for the drop ejection by the microvalve under examination is sufficient to overcome the surface tension at a moderate Weber number and to form a droplet.[39] Therefore, these specifications were assumed for the simulation of both techniques, ADE and DoD. The Weber numbers in the simulation were calculated as 10.64 for DoD and 4.16 for ADE based on water at standard conditions, and the droplet diameter was chosen as the characteristic length rather than the conventionally used nozzle diameter in order to better compare DoD and ADE. Based on the simulation results (Figure 3b,c,e,f and Video S4, Supporting Information), the maximum shear stress induced by nozzle-based DoD printing using the aforementioned microvalve is approximately three times higher than the maximum shear stress during ADE process. If smaller drop sizes are required a decrease in valve size is required, which will inevitably result in even higher shear stress when using the DoD inkjet bioprinting method. This analysis proves that by using ADE, the absence of a nozzle assures lower maximum shear stress during droplet ejection compared to nozzle-based DoD. From the mechanical point of view, therefore, ADE offers potential for cell-preserving bioprinting while simultaneously maintaining higher printing resolution.

To prove this, printability tests of ADE were performed using several different materials and two different cell types. The tested materials were 7.5% gelatin and 1% agarose (both at 37 °C), and Pluronic F-127 and Matrigel (both at 7 °C), all of which exhibit different viscosities and surface tension. Although the printing results with gelatin and agarose are not presented here, the experiments with 7.5% gelatin and 1% agarose indicated an upper limit in hydrogel concentration. This supports the general principle that viscosity and surface tension limit the material range, thus having a direct effect on printability and droplet size. The setup contains an integrated cooling and heating system that ensures a constant temperature of either 7 or 37 °C. The reservoir maintains the printing materials in their liquid phase, while the independent temperature setting at the building platform favors the gelation process of the printed material. In this way, a hollow Pluronic cylinder with an outer diameter of 6 mm and a height of 1.6 mm was printed on a Ø12 mm glass coverslip using ADE (**Figure 4**a). The Pluronic viscosity was 0.03 Pas at shear rates higher than 20 s^{-1} (Figure S8, Supporting Information). The drop pattern of the cylinder consisted of 96 drops in 15 layers. To improve the stability of the hollow structure, the cylinder was made of two droplets deposited in a radial direction, resulting in a wall thickness of 0.6 mm. In order to achieve higher build-ups the axis repetition accuracy must be improved, and at a certain height the temperature control will no longer be efficient. The current printing rig was optimized for a glass coverslip 12 mm in diameter, which could be extended to a larger printing area in the future.

The potential negative effects of the ADE method on living cells were tested first by using MG-63 osteosarcoma cell line embedded in Pluronic. A structure of 96 droplets was printed and effects on cell viability, morphology, and prodifferentiation capacities were examined. No negative impact on cell survival was found in either of the tested samples, whether ADE-printed or nonprinted. Both experimental settings showed more than 90% of alive cells immediately after manipulation (Figure 4b). This result confirms that the energy contained in the focused sound that is needed to produce drops is far below cell-damaging intensities.[40] The long-term effects of ADE bioprinting on cell behavior were evaluated by examining the organization, adhesive, and prodifferentiation capacities of an additional cell type. More sensitive primary human mesenchymal stem cells (MSCs) were selected for the ADE bioprinting after embedding in two different hydrogels, Pluronic and Matrigel. After the printing process, these were placed in a well and medium was added to dissolve the Pluronic hydrogel. No differences in MSC distribution between ADE and non-ADE samples were found (Figure 4c,d). In addition, immunofluorescence staining with phalloidin (F-actin; green signal) confirmed no variability in stress fiber organization. Distribution of focal adhesions (Vinculin; red spots) was also compared (Figure 4c) and confirmed that ADE did not negatively affect the capacity of cells to adhere to the plate. Similarly, the prodifferentiation capacities of MSCs toward osteoblast lineage were maintained in ADE samples, which showed identical patterns of calcium deposition (Alizarin; red staining) compared to the non-ADE printed controls (Figure 4d). Finally, the same characteristics were confirmed in 3D structures obtained by ADE bioprinting of MSC embedded in Matrigel. The cells were equally distributed within the gel, showing typical mesenchymal morphology (Figure 4e). The tight cell-to-cell interaction resulted in a meshwork-like cell organization instead of the flat distribution observed in 2D conditions (Figure 4c). The analysis was performed 7 d post ADE bioprinting, confirming the excellent biocompatibility and printability of a Matrigel hydrogel.

In summary, using the ADE method a novel technique is introduced by which cell-laden hydrogel structures can be 3D bioprinted with a high degree of precision. This 3D assembly of solidified droplets marks a new development for the ADE field. The simulation results confirm that ADE guarantees much lower shear stress on the printed cells compared to the established DoD bioprinting technique using microvalves. This is further confirmed by the fact that the cells embedded in the hydrogel structures exhibited neither a loss in viability nor any negative long-term effects. Furthermore, the ADE technology enables the generation of variable droplet size over more than three length scales, with droplet sizes from the millimeter length scale down to the size of a single cell. This enables the tailoring of the droplet size by simply changing the acoustic wave frequency and without the need for time-consuming hardware exchange. By modulating the frequency, amplitude and corresponding signal duration, it is possible to tailor droplet formation without the risk of satellite droplets. Therefore, the presented multiscale and cell-preserving bioprinting method

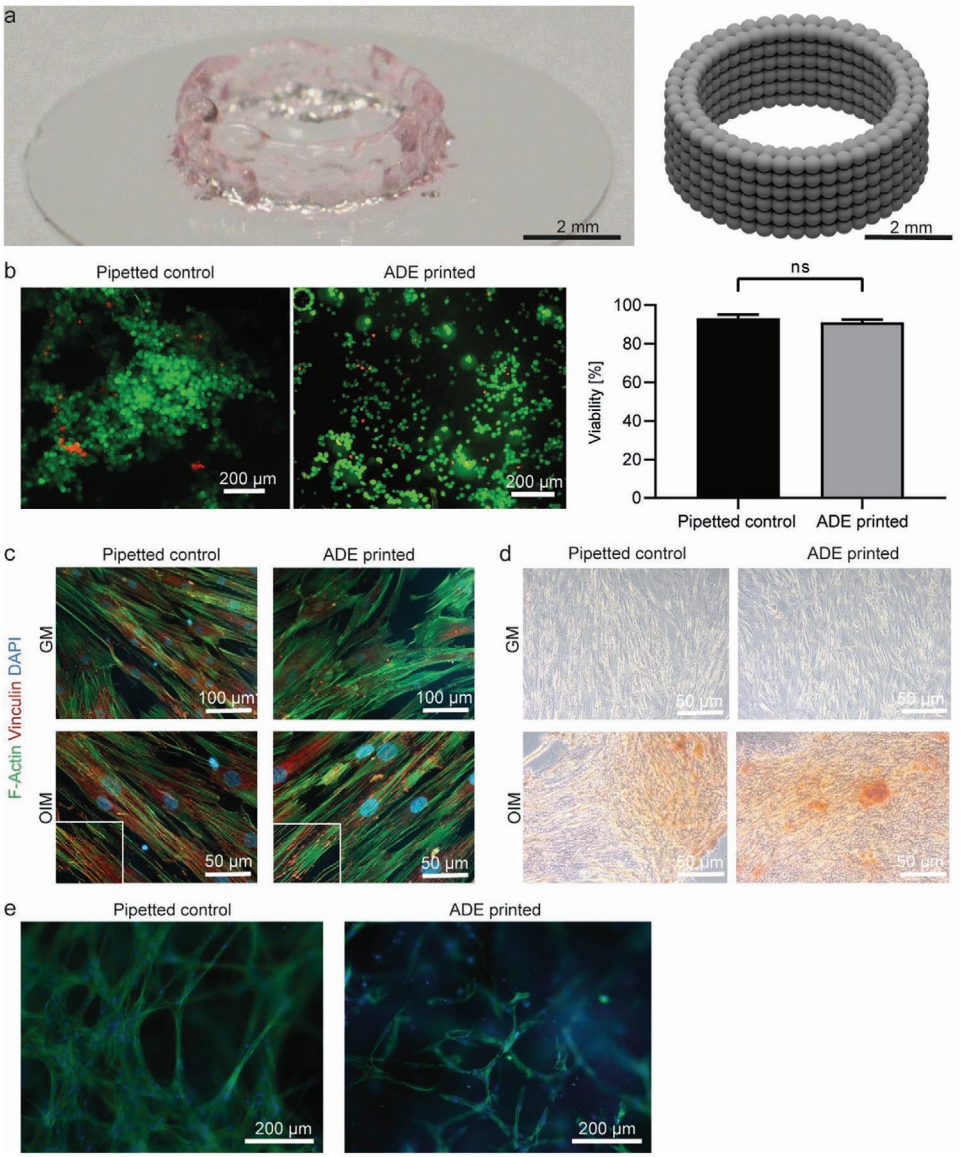

Figure 4. Proof of acoustic droplet ejection (ADE) 3D bioprintability. a) A cylinder consisting of 96 droplets per layer was printed. b) Cell viability was evaluated by FDA (green; alive cells) and PI (red; dead cells) staining. Three independent measurements were performed. Graph bars show the mean (±standard deviation) percentage of alive cells in ADE printed or pipetted control sample. Scale bar: 200 µm. n.s.—nonsignificant. c) Representative images of cell organization and stress fibers distribution (green) are shown. Vinculin antibody was used to visualize focal adhesions (red). Insets show magnification of MSC focal adhesions. DAPI (blue) served for nuclei staining. Scale bars: 100 and 50 µm. d) Alizarin red staining of the MSCs grown in Mesenpan (growth medium; GM) and osteoinductive medium (OIM) for 14 d is shown. Comparison of ADE and pipetted control samples. Scale bar: 50 µm. e) Distribution of MSCs embedded in Matrigel hydrogel after 7 d of growth was analyzed. Representative images of MSC organization within the Matrigel and stress fiber distribution (green) are shown for ADE bioprinted and pipetted control samples. DAPI was used for nuclear staining. Scale bars: 200 µm.

has great potential for 3D tissue engineering, regenerative medicine, and mechanobiology.

Experimental Section

Ultrasonic Setup: A US-Key Single Channel Ultrasound Device (Lecoeur Electronique) was used to determine the focus position of the HIFU transducer. The circuit for the printing process was then modified as explained with two different transducers. The approximate frequencies were taken from a measurement of the reflection coefficient (Figure S3, Supporting Information). Due to the imperfect coupling between mechanical resonance and electrical resonance, the frequencies that were finally used had a slight offset. The first transducer was used at 4.60 and 13.60 MHz. The second transducer was used at 7.01 MHz.

Droplet Acquisition: The acquisition was performed with a 5 megapixel camera (VCXU-51M, Baumer) and a 3.2 megapixel camera (acA2040-120um, Basler), each with the same objective (FL-BC7528-9M, Ricoh). A spot illumination (SpotOne, Büchner Lichtsysteme) in combination with an light-emitting diode (LED) strobe controller (HPSC1, Smartek) was used. The LED strobe controller was triggered by the second channel of

a waveform generator (33612A, Keysight). The ejection at 7.01 MHz was performed at the fundamental frequency with another HIFU transducer (PZT-82, 19.5 mm, 7 MHz, Zibo Yuhai Electronic Ceramic).

Preparation of Bioinks: Pluronic F-127 powder (P2443, Sigma-Aldrich) was mixed in a ratio of 25% w/v and 30% w/v with 4 °C cold Mesenpan culture medium (P08-50400K, PAN-Biotech). The solution was mixed for 2 h at 4 °C using a roller mixer. Bone marrow derived MSCs were isolated from human bone marrow aspirate, which was consented to and followed the guidelines of the Ethics Committee of the Faculty of Medicine of RWTH Aachen University (EK 300/13). The MSCs were added to a final cell concentration of 5 million cells per mL. Matrigel High Concentration growth factor reduced and lactose dehydrogenase elevating virus free (354263, Corning Life Science) was diluted with Mesenpan culture medium (P08-50400K) at a temperature of 4 °C, to a protein concentration of 10 mg mL^{-1}. Adipose derived stem cells were mixed with the diluted Matrigel to a final cell concentration of 2 million cells per mL.

Medium for Cell Cultivation: Mesenpan culture medium (P08-50400K) was supplemented with 2% v/v fetal bovine serum (26140079, Thermo Fisher Scientific) and 1% v/v penicillin/streptomycin (15140122, Thermo Fisher Scientific) for nondifferentiated cells. For the osteogenic stimulation, MSCs were grown in dulbecco's modified Eagle medium - low glucose (D6046, Sigma Aldrich) supplemented with 10% v/v fetal bovine serum (26140079, Thermo Fischer Scientific), 1% v/v penicillin/streptomycin (15140122, Thermo Fisher Scientific), 100×10^{-9} M dexamethasone (D4902, Sigma-Aldrich), 10×10^{-3} M beta-glycerophosphate (G9422, Sigma-Aldrich), and 0.05×10^{-9} M L-ascorbic acid-2-phosphate (A8960, Sigma-Aldrich). Calcium deposits in osteogenic-differentiated MSCs were evaluated by Alizarin red staining as described previously.[41] Live/dead staining was performed using a fluorescein diacetate (FDA) and propidiumiodide (PI) assay (F7378-10G/P4170-10116, SIGMA Life Science) and image acquisition was done immediately after as described in the cell microscopy section below. The results were analyzed using Fiji open source software.

Cell Microscopy: Immunofluorescence pictures were taken with Axio Imager 2 microscope (Zeiss) and Zeiss Efficient Navigation software (Zeiss). Samples were prepared by fixing them in 4% formaldehyde for 10 min (2D) and 30 min (3D). This step was followed by cell permeabilization with the solution of 0.1% of TritonX-100 in 1xPBS (5 min (2D), 30 min (3D)), and incubation in 3% bovine serum albumin of blocking solution for 30 min (2D and 3D). Subsequently, the samples were incubated overnight at 4 °C with Alexa Fluor 488 Phalloidin (A12379, Thermo Fisher Scientific, excitation/emission 495/518 nm, 1:250) and with an anti-Vinculin primary antibody (14-9777-82, Thermo Fisher Scientific, 1:5000). Next, incubation with conjugated secondary antibody Alexa Fluor 555 (A-31570, Thermo Fisher Scientific, excitation/emission 555/567, 1:2000) was performed for 60 min (2D) and 90 min (3D) at room temperature, and the nuclei were counterstained with 4′,6-diamidino-2-phenylindole (DAPI) (1:3000, Thermo Fisher Scientific (for 3D) and ProLong Gold Antifade with DAPI, P36941, Thermo Fisher Scientific (for 2D)).

Printing Process: The hydrogels were tempered to 7 °C inside the printing reservoir. For printing Pluronic, the building platform was heated to 37 °C. If Matrigel was used, the building platform was at room temperature (≈23 °C). The ultrasonic system had an impedance of 50 Ω. For printing 25% w/v Pluronic, the signal had a peak-to-peak amplitude of 190 mV (+ 50 dB = 60.06 V ≙ 9.02 W) and 190 cycles (≙ 41.3 µs excitation length) at a frequency of 4.6 Mhz. Signal parameters for printing Matrigel (10 mg mL^{-1} protein concentration) was set to a peak-to-peak amplitude of 170 mV (+ 50 dB = 53.76 V ≙ 7.23 W), 160 Cycles (≙ 35.2 µs excitation length) at a frequency of 4.55 MHz. Between each printed droplet there was a minimum delay of 300 ms. The droplet layers were printed on round coverslips 12 millimeter in diameter and 1 mm in thickness (Carl Roth) made of borosilicate glass from hydrolytic class 1. The cultivation and imaging were performed directly on the glass coverslips.

Numerical Simulation: ANSYS CFX 19.2 was used for all of the numerical simulations. This software uses FEM to solve the governing equations. For this simulation, the fluid was considered incompressible, isothermal conditions were imposed, and the maximum root-mean-square residual error of 10^{-4} was chosen. Nonuniform mesh with higher mesh density in the areas of expected high gradients was used. To ensure the use of proper element size, the grid study was performed on three different mesh sizes for ADE and four different mesh sizes for DoD considering the sensitive parameters (maximum water velocity for the acoustic droplet ejection and wall shear stress for DoD). To reduce the computational cost, the second finest meshes were applied in further studies for ADE and DoD.

For the acoustic droplet ejection, an axisymmetric domain was considered. For such a problem, the governing equations to be solved were continuity, momentum, and volume fraction coupling equations. The liquid–air interface was modeled based on free surface model and constant force along the interface. The acoustic wave effect was modeled as a volumetric momentum source added to the momentum equations.[37,38] An adaptive time step size based on maximum courant number was set and the effect of time step size was studied to ensure the stability and accuracy of the performed simulation. The total simulation time of 2.0 ms was considered. For the DoD, the 90° symmetric geometry was used and the fluid flow inside the valve was simulated. For such a problem, the governing equations are continuity and momentum equations. Transient simulation within the valve opening time (500 µs) was considered and the total flow rate during this time (drop volumetric size) was validated with previous experimental measurements.[34] The necessary analysis that the simulation results are independent of mesh and time step size was performed and reported in the Supporting Information.

Supporting Information

Supporting Information is available from the Wiley Online Library or from the author.

Acknowledgements

The authors acknowledge the financial support from the Deutsche Forschungsgemeinschaft (DFG, German Research Foundation)—423054768/FI 975/32-1 and 363055819/GRK2415.

Open access funding enabled and organized by Projekt DEAL.

Conflict of Interest

The authors declare no conflict of interest.

Data Availability Statement

Research data are not shared.

Keywords

3D bioprinting, acoustic droplet ejection, human cells, multiscale printing, tissue engineering

Received: October 14, 2020
Revised: February 3, 2021
Published online: May 4, 2021

[1] K. Bardsley, A. J. Deegan, A. El Haj, Y. Yang, *Adv. Exp. Med. Biol.* **2017**, *1035*, 3.

[2] W. Sun, B. Starly, A. C. Daly, J. A. Burdick, J. Groll, G. Skeldon, W. Shu, Y. Sakai, M. Shinohara, M. Nishikawa, J. Jang, D.-W. Cho, M. Nie, S. Takeuchi, S. Ostrovidov, A. Khademhosseini,

R. D. Kamm, V. Mironov, L. Moroni, I. T. Ozbolat, *Biofabrication* **2020**, *12*, 022002.
[3] S. V. Murphy, A. Atala, *Nat. Biotechnol.* **2014**, *32*, 773.
[4] C. M. Smith, A. L. Stone, R. L. Parkhill, R. L. Stewart, M. W. Simpkins, A. M. Kachurin, W. L. Warren, S. K. Williams, *Tissue Eng.* **2004**, *10*, 1566.
[5] R. Chang, J. Nam, W. Sun, *Tissue Eng., Part A* **2008**, *14*, 41.
[6] K. Nair, M. Gandhi, S. Khalil, K. C. Yan, M. Marcolongo, K. Barbee, W. Sun, *Biotechnol. J.* **2009**, *4*, 1168.
[7] S. Datta, A. Das, A. R. Chowdhury, P. Datta, *Biointerphases* **2019**, *14*, 051006.
[8] J. Bohandy, B. F. Kim, F. J. Adrian, *J. Appl. Phys.* **1986**, *60*, 1538.
[9] J. A. Barron, B. R. Ringeisen, H. Kim, B. J. Spargo, D. B. Chrisey, *Thin Solid Films* **2004**, *453–454*, 383.
[10] M. Gruene, C. Unger, L. Koch, A. Deiwick, B. Chichkov, *Biomed. Eng. Online* **2011**, *10*, 19.
[11] N. T. Kattamis, P. E. Purnick, R. Weiss, C. B. Arnold, *Appl. Phys. Lett.* **2007**, *91*, 171120.
[12] S. Michael, H. Sorg, C.-T. Peck, L. Koch, A. Deiwick, B. Chichkov, P. M. Vogt, K. Reimers, *PLoS One* **2013**, *8*, e57741.
[13] T. Xu, C. A. Gregory, P. Molnar, X. Cui, S. Jalota, S. B. Bhaduri, T. Boland, *Biomaterials* **2006**, *27*, 3580.
[14] H. Gudapati, M. Dey, I. Ozbolat, *Biomaterials* **2016**, *102*, 20.
[15] U. Demirci, G. Montesano, *Lab Chip* **2007**, *7*, 1139.
[16] Y. Fang, J. P. Frampton, S. Raghavan, R. Sabahi-Kaviani, G. Luker, C. X. Deng, S. Takayama, *Tissue Eng., Part C* **2012**, *18*, 647.
[17] R. Ellson, M. Mutz, B. Browning, L. Lee Jr, M. F. Miller, R. Papen, *J. Assoc. Lab. Autom.* **2003**, *8*, 29.
[18] U. Demirci, *J. Microelectromech. Syst.* **2006**, *15*, 957.
[19] H. F. Bok, W. R. Johnson, J. P. O'Connor, M. M. Shade, L. D. Young, *US 5,669,971*, **1997**.
[20] B. Hadimioglu, S. Elrod, R. Sprague, in *IEEE Ultrasonics Symposium. Proceedings*, IEEE, Atlanta, GA **2001**, p. 627.
[21] C.-Y. Lee, H. Yu, E. S. Kim, in *TRANSDUCERS – International Solid-State Sensors, Actuators and Microsystems Conference*, IEEE, Lyon, France **2007**, p. 1283.
[22] S. A. Elrod, B. Hadimioglu, B. T. Khuri-Yakub, E. G. Rawson, C. F. Quate, N. N. Mansour, T. S. Lundgren, in *AIP Conference Proceedings*, IEEE Ultrasonics Symposium Proceedings, Chicago, IL **1988**, p. 699.
[23] C. F. Quate, B. T. Khuri-Yakub, *Nozzleless Liquid Droplet Ejectors*, *US Patent 4,697,195*, **1987**.
[24] E. Tekin, P. J. Smith, U. S. Schubert, *Soft Matter* **2008**, *4*, 703.
[25] S. A. Elrod, B. Hadimioglu, B. T. Khuri-Yakub, E. G. Rawson, E. Richley, C. F. Quate, N. N. Mansour, T. S. Lundgren, *J. Appl. Phys.* **1989**, *65*, 3441.
[26] G. R. Torr, *Am. J. Phys.* **1984**, *52*, 402.
[27] R. W. Wood, A. L. Loomis, *London, Edinburgh, Dublin Philos. Mag. J. Sci.* **1927**, *4*, 417.
[28] Z. Ma, A. W. Holle, K. Melde, T. Qiu, K. Poeppel, V. M. Kadiri, P. Fischer, *Adv. Mater.* **2020**, *32*, 1904181.
[29] C. Bouyer, P. Chen, S. Güven, T. T. Demirtaş, T. J. F. Nieland, F. Padilla, U. Demirci, *Adv. Mater.* **2016**, *28*, 161.
[30] D. Petta, V. Basoli, D. Pellicciotta, R. Tognato, J. P. Barcik, C. Arrigoni, E. D. Bella, A. R. Armiento, C. Candrian, G. R. Richards, M. Alini, M. Moretti, D. Eglin, T. Serra, *Biofabrication* **2020**, *13*, 015004.
[31] J. W. S. Rayleigh, *The Theory of Sound*, Vols. I and II, Dover Publications, Newburyport **1945**.
[32] A. Shafiee, E. Ghadiri, H. Ramesh, C. Kengla, J. Kassis, P. Calvert, D. Williams, A. Khademhosseini, R. Narayan, G. Forgacs, A. Atala, *Appl. Phys. Rev.* **2019**, *6*, 021315.
[33] J. Schöneberg, F. de Lorenzi, B. Theek, A. Blaeser, D. Rommel, A. J. C. Kuehne, F. Kießling, H. Fischer, *Sci. Rep.* **2018**, *8*, 10430.
[34] A. Blaeser, D. F. Duarte Campos, U. Puster, W. Richtering, M. M. Stevens, H. Fischer, *Adv. Healthcare Mater.* **2016**, *5*, 326.
[35] T. Boland, T. Xu, B. Damon, X. Cui, *Biotechnol. J.* **2006**, *1*, 910.
[36] M. Betsch, C. Cristian, Y.-Y. Lin, A. Blaeser, J. Schöneberg, M. Vogt, E. M. Buhl, H. Fischer, D. F. Duarte Campos, *Adv. Healthcare Mater.* **2018**, *7*, 1800894.
[37] B. Moudjed, V. Botton, D. Henry, H. Ben Hadid, J.-P. Garandet, *Phys. Fluids* **2014**, *26*, 093602.
[38] G. Launay, T. Cambonie, D. Henry, A. Pothérat, V. Botton, *Phys. Rev. Fluids* **2019**, *4*, 044401.
[39] B. Derby, *Annu. Rev. Mater. Res.* **2010**, *40*, 395.
[40] B. Hadimioglu, R. Stearns, R. Ellson, *J. Lab. Autom.* **2016**, *21*, 4.
[41] S. Aveic, R. Davtalab, M. Vogt, M. Weber, P. Buttler, G. P. Tonini, H. Fischer, *Acta Biomater.* **2019**, *88*, 527.